Effect of higher-order multipole moments on the Stark line shape

T. A. Gomez, T. Nagayama, D. P. Kilcrease, M. H. Montgomery, and D. E. Winget

The Effect of Higher-Order Multipole Moments on the Stark Line Shape

T.A. Gomez,[1, *] T. Nagayama,[2] D.P. Kilcrease,[3] M.H. Montgomery,[1] and D. E. Winget[1]

[1]*University of Texas at Austin*
[2]*Sandia National Laboratories*
[3]*Los Alamos National Laboratories*
(Dated: July 7, 2016)

Spectral line shapes are sensitive to plasma conditions and are often used to diagnose electron density of laboratory plasmas as well as astrophysical plasmas. Stark line-shape models take into account the perturbation of the radiator's energy structure due to the Coulomb interaction with the surrounding charged particles. Solving this Coulomb interaction is challenging and is commonly approximated via a multipole expansion. However, most models include only up to the second term of the expansion (the dipole term). While there have been studies on the higher-order terms due to one of the species (i.e., either ions or electrons), there is no model that includes the terms beyond dipole from both species. Here, we investigate the importance of the higher-order multipole terms from both species on the Hβ line shape. First, we find that it is important to include higher-order terms consistently from both ions and electrons to reproduce measured line-shape asymmetry. Next, we find that the line shape calculated with the dipole-only approximation becomes inaccurate as density increases. It is necessary to include up to the third (quadrupole) term to compute the line shape accurately within 2%. Since most existing models include only up to the dipole terms, the densities inferred with such models are in question. We find that the model without the quadrupole term slightly underestimates the density, and the discrepancy becomes as large as 12% at high densities. While the case of study is limited to Hβ, we expect similar impact on other lines.

I. INTRODUCTION

In a dense plasma, the bound electrons of every ion and/or atom is perturbed by its nearby charged particles, which affects its line transition energies and widths. The ensemble effect of this random perturbation is observed as the spectral line broadening. As density increases, the perturbations become stronger, and the spectral line shape broadens in a complex way, making detailed line-shape modeling a challenging enterprise. Nevertheless, the line shape remains a powerful and precise tool to diagnose laboratory and astrophysical plasmas [1–3].

In a dense plasma, the Hamiltonian of a hydrogen atom can be expressed (with the nucleus at $\vec{r} = 0$; atomic units throughout: $\hbar = 1, e = 1, m_e = 1$) as:

$$H(t) = H_0(t) + V_{\text{ext}}(\vec{r}, t), \tag{1}$$

$$H_0(t) = -\frac{1}{2}\nabla^2 - \frac{1}{|\vec{r}|}, \tag{2}$$

where $H_0(t)$ is the Hamiltonian for the unperturbed hydrogen and $\vec{r}$ is the position operator of the radiator electron. $V_{\text{ext}}(\vec{r}, t)$ is the time-dependent perturbing Coulomb potential due to the surrounding charged particles (protons and electrons):

$$V_{\text{ext}}(\vec{r}, t) = \sum_j^N \left[\frac{q_j}{|\vec{R}_j(t)|} - \frac{q_j}{|\vec{r} - \vec{R}_j(t)|} \right], \tag{3}$$

where the first and second terms in the summation are the Coulomb potential energies due to the perturber j on the nucleus (at origin) and the bound electron, respectively; the sum is over the N particles interacting with the radiator (bound electron plus nucleus). The origin is chosen to be nucleus of the radiator. The charge and time-dependent position of perturber j are denoted as q_j and $\vec{R}_j(t)$, respectively. In general, Eq. (3) is not exactly solvable due to complexities [4] of the many-body problem and therefore must be treated approximately.

One common approach to handle this many-body problem is to use multipole expansion of Eq. (3) about the nucleus of the radiator [4, 5]; this expands the contribution from each perturber j, assuming the perturbing particles are outside the radiating atom [1]:

$$\frac{q_j}{|\vec{R}_j(t)|} - \frac{q_j}{|\vec{r} - \vec{R}_j(t)|} = \frac{q_j}{R_j(t)} - \left[\frac{q_j}{R_j(t)} \right.$$
$$\left. + \frac{q_j r}{R_j^2(t)} \cos\gamma_j(t) + \frac{q_j r^2}{R_j^3(t)}(3\cos^2\gamma(t) - 1) \cdots \right]$$
$$= -\sum_{k=1}^{\infty} q_j \frac{r^k}{R_j^{k+1}(t)} P_k(\cos\gamma_j(t)), \tag{4}$$

where the brackets contain the Taylor expansion of the bound-electron term; $r \equiv |\vec{r}|$, $R_j(t) \equiv |\vec{R}_j(t)|$, $\gamma_j(t)$ is the angle between $\vec{r}$ and $\vec{R}_j$, and $P_k(x)$ are Legendre polynomials [4]. The first ($k = 0$), second ($k = 1$),

---

* gomezt@astro.as.utexas.edu

[1] Replace $r^k/R_j^{k+1}(t)$ with $\min[r, R_j(t)]^k/\max[r, R_j(t)]^{k+1}$ for a more general expression [5].

and third ($k = 2$) terms are called monopole, dipole, and quadrupole, respectively, and correspond to the electric potential, the electric field, and the gradient of the electric field at the nucleus of the radiator produced by perturber j. While we derive Eq. (4) only for neutral hydrogen for our application, the perturbation potential due to nearby charged particles can always be expressed in multipole expansion for any radiator (i.e., neutral or charged, single or multiple bound electrons). Thus, the concern associated with the use of multipole expansion is general to any line-shape model.

Most line-shape broadening calculations evaluate Eq. (4) out to only the dipole term [6–9], which produces the Stark effect. There have been only a limited number of studies that have included terms higher than the dipole term. Moreover, those studies investigated the effect of the higher-order terms only due to either ions [10–12] or electrons [13, 14]. To our knowledge, no calculation simultaneously includes higher-order terms from both ions and electrons.

In this paper, we investigate the impact of terms beyond the dipole term from both ion and electrons using a particle-simulation method. We are particularly interested in the hydrogen Balmer-β (Hβ) line shape due to its application for white dwarf star and laboratory diagnostics [3]. In Sec. 2, we describe the simulation-based line-shape model used in this article. For the first time, we include the higher-order multipole terms from both ions and electrons simultaneously. In Sec. 3, we find that the electron quadrupole term is as important as the ion quadrupole term to accurately model asymmetry near the Hβ line center. We perform a line-shape convergence study in Sec. 4 that includes up to the sedecapole ($k = 4$) term and study how many terms are necessary to accurately model Hβ. We find that the quadrupole term becomes important at densities as low as one order of magnitude below the Inglis-Teller limit [15]. Since Hβ is often used as a plasma diagnostic, Sec. 5 further investigates its impact on the inferred electron density, n_e. At low density ($n_e \leq 10^{17}$ electrons per cubic centimeter; e/cc), the line shape calculated only up to the dipole term is sufficiently accurate. However, at higher density ($n_e \sim 10^{18}$ e/cc), the inferred density is underestimated by 15%. Sec. 6 summarizes our conclusions.

II. CALCULATIONAL CONSIDERATIONS

The line shape is defined as the Fourier transform of the average dipole autocorrelation function [16],

$$L(\omega) = \int_0^\infty e^{i\omega t} \sum_{\alpha\beta} \rho_\alpha \vec{D}_{\beta\alpha} \cdot \langle U(t)\vec{D}_{\alpha\beta}U^\dagger(t)\rangle_{\mathrm{av}} dt, \quad (5)$$

where initial and final states of the transition are denoted by α and β, respectively; $\langle\rangle_{\mathrm{av}}$ denotes an ensemble average over perturber configurations; ρ_α is the population of the initial state; $\vec{D}_{\alpha\beta}$ is the dipole moment that

connects the initial state to the final state; and $U(t)$ is the time-evolution operator, which is the solution to the time-dependent Schrödinger equation,

$$i\frac{d}{dt}U(t) = H(t)U(t), \quad (6)$$

where the Hamiltonian includes a time-dependent interaction potential due to the perturbing particles as shown in Eq. (1)-(4). This line-shape formula, Eq. (5), can be evaluated using two primary approaches: i) the analytic approach, known as standard theory [6, 7], and ii) the particle-simulation approach [8, 9]. While the analytic approach is quite fast, it introduces approximations that are not needed in the simulation approach. Also, while it is more straightforward to include electron/ion higher-order terms in the simulation, the importance of higher-order terms has never been investigated with the simulation approach. Thus, we use a simulation-based line-shape model throughout this article.

In the simulation approach, $H(t)$ is computed with Eq (1)-(4) by simulating the motions of all the perturbers around the radiator. Then, $U(t)$ is solved with Eq. (6), which is used to compute the time development of the dipole operator, $U(t)\vec{D}_{\alpha\beta}U^\dagger(t)$. This calculation is repeated with different randomness in the perturber motions, and its configurational average, $\left\langle U(t)\vec{D}_{\alpha\beta}U^\dagger(t)\right\rangle_{\mathrm{av}}$, is simulated. Finally, the line shape is computed by numerically integrating Eq. (5), which is explained in detail in [17, 18].

We treat perturbing particles classically. This assumption is commonly made in simulation line-shape calculations and is valid when the average inter-particle distance is much greater than the thermal de Broglie wavelength [19]. All the cases we explore in this article have characteristic inter-particle distances greater than 4 de Broglie wavelengths.

For our study, we approximate the perturber motions with straight-path trajectories [2]. This approximation neglects the Coulomb forces of the perturbers on each other. Stambulchik *et al.* [20] showed that the effect of the perturber-perturber interaction can be approximated with the Debye-screened Coulomb potential for weakly coupled plasmas. To take this into account, we introduce a Debye screening factor to Eq. (3):

$$V_{\mathrm{ext}}(\vec{r}, t) = \sum_j q_{ij} \left[\frac{q_j}{|\vec{R}_j(t)|} e^{-|\vec{R}_j(t)|/\lambda_\mathrm{D}} \right.$$
$$\left. - \frac{q_j}{|\vec{r} - \vec{R}_j(t)|} e^{-|\vec{r} - \vec{R}_j(t)|/\lambda_\mathrm{D}} \right], \quad (7)$$

---

[2] If the net charge of the radiator were non-zero, the perturbing particles would follow hyperbolic trajectories around a Coulomb potential of charge ($Z - N_b$) where Z is the charge of the nucleus and N_b is the number of bound electrons.

where $\lambda_{\mathrm{D}} = \sqrt{k_B T/4\pi n_e}$ is the electron Debye length. The resulting Taylor expansion of the screened Coulomb potential is Eq. (4) multiplied by the exponential screening factor and a polynomial S_k [3]:

$$V_{\mathrm{ext}}(\vec{r},t) = -\sum_j \sum_{k=1}^{\infty} q_j \frac{r^k}{R_j^{k+1}(t)} P_k(\cos\gamma_j(t)) \times$$
$$S_k(R_j(t)/\lambda_{\mathrm{D}}) e^{-R_j(t)/\lambda_{\mathrm{D}}}, \qquad (8)$$

where $S_k(x)$ comes from the Debye screening factor:

$$S_0(x) = 1$$
$$S_1(x) = 1 + x$$
$$S_2(x) = 1 + x + \frac{1}{3}x^2$$
$$S_3(x) = 1 + x + \frac{2}{5}x^2 + \frac{1}{15}x^3$$
$$S_4(x) = 1 + x + \frac{1}{9}x^2 + \frac{4}{81}x^3 + \frac{1}{81}x^4$$
$$\vdots \qquad (9)$$

At higher coupling parameters, the trajectories of classical particles are no longer accurately described by the Debye-screened straight paths and perturber motions need to be computed in detail taking into account Coulomb interactions. Stambulchik *et al.* [20] demonstrated how this alters the effective screening length of the electrons, increasing it beyond what is predicted by the Debye theory. However, the errors in the effective screening length mostly influence long-range interaction, which is dominated by the lowest-order terms (e.g., dipole term). Thus, we expect that detailed treatment of perturber motions would mostly impact the accuracy of the dipole term and not our conclusions on the importance of the higher-order terms.

One advantage in using the screened Coulomb potential is that particles beyond a few Debye lengths are completely screened and do not contribute to the line shape. Therefore, the total number of particles in our simulation (Eq. 3) is determined by the conditions of our plasma. We performed a sensitivity study and chose the simulation box to be at least 5 Debye lengths. The number of the particles used in the simulation is based on the box size and the particle number density. If, however, we perform a fully-interacting simulation (as opposed to the non-interacting simulation), then we may require several thousand particles in a much bigger box.

Finally, we make a note on the basis set (number of elements of the state vector) required for accurate quantum-mechanical calculation. We perform the $U(t)\vec{D}_{\alpha\beta}U^\dagger(t)$

---

[3] Additional terms that are of lower-order angular dependence are ignored. For example, the Taylor expansion for $k = 2$ is $[P_2(\cos\gamma)r^2 S_2(R/\lambda_{\mathrm{D}})/R^3 + r^2(R/\lambda_{\mathrm{D}})^2/6R^3]\exp(-R/\lambda_{\mathrm{D}})$, and we are ignoring the second term in brackets, which is the divergence term; this is commonly assumed to be zero inside the radiator wavefunction [12]
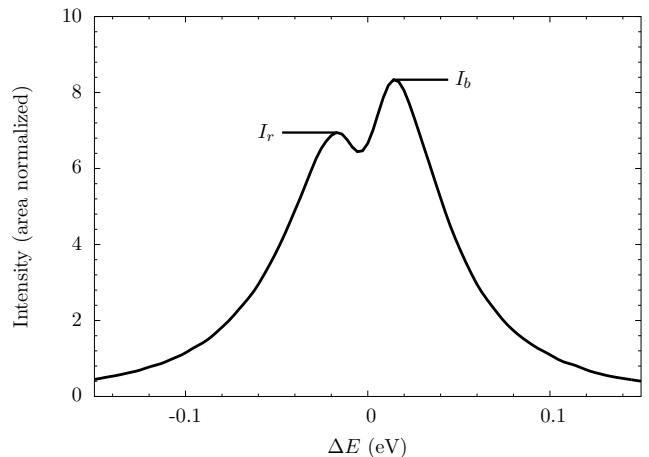

FIG. 1. The double-peaked Hβ line shape. The asymmetry of the core is defined as the fractional difference of the intensity of the blue peak and red peak, $(I_b - I_r)/I_b$, where the subscripts b and r denote the blue ($\Delta E > 0$) and red peak ($\Delta E < 0$), respectively.

calculation with a matrix representation of operators and states; accuracy of perturbed atomic structure depends on the choice of the basis set included in this representation. Most previous calculations include only the states in the same shell as the upper and lower states of the transition. For example, for Hβ, only $2s$, $2p$, $4s$, $4p$, $4d$, and $4f$ are included. When the perturbation is small, a linear combination of these states accurately represents the perturbed states. However, as n_e increases, $n = 4$ states start to mix with $n = 5$ states, and the next manifold (i.e., $5s$, $5p$, $5d$, $5f$, and $5g$) needs to be added to the basis set to accurately compute the Hβ line shape. The importance of this extended basis set has been confirmed previously [10, 20, 21], and we use this extended basis set for the rest of the article.

III. THE ELECTRON QUADRUPOLE MOMENT AND THE Hβ ASYMMETRY

Griem [22] considered the quadrupole term due to the ions (denoted as Q_i and often referred to as the ion quadrupole in the literature) as a primary source of asymmetry in Hβ. More recent studies have shown that the mixing of state n with state $n + 1$ (i.e., an expanded basis) is also a source of asymmetry [10, 20]. Djurović *et al.* [21] studied extensively the effects of asymmetry in the Hβ line by introducing the extended basis set to the simulation-based line-shape model and by introducing the ion quadrupole effect to the semi-analytic theory. The simulation model was able to reproduce the measured asymmetry for densities below a few 10^{17} e/cc, but over-predicted the asymmetry above this threshold. The semi-analytic model was able to match the measurements above this same threshold, but not be-

low. No single calculation was able to match the data over the entire density range presented in Djurović *et al.* ($1 \times 10^{16} - 1.2 \times 10^{18}$ e/cc).

Here, we revisit this study of Hβ asymmetry with the new simulation-based model developed in Sec. II. We include not only the extended basis set and the ion quadrupole term but also the electron quadrupole term, Q_e. We focus our attention on a smaller range of densities, $n_e = 1 \times 10^{17} - 1.2 \times 10^{18}$ e/cc, where there is discrepancy with the simulation calculation of Djurović *et al.* [21]. We compute the Hβ line shapes with three different descriptions of higher-order terms: 1) dipole terms only for both ions and electrons, denoted as $D_i + D_e$, and 2) up to quadrupole terms for ions but dipole terms only for the electrons, denoted as $Q_i + D_i + D_e$, and 3) up to quadrupole terms for both ions and electrons, denoted as $Q_i + Q_e + D_i + D_e$. Note that the extended basis set is used for all the three cases. The asymmetry of the calculated line shape is defined in the same way as Djurović *et al.* [21], which is the ratio of the difference of the blue ($\Delta E > 0$, where $\Delta E = 0$ is the unshifted Hβ photon energy) and red peak ($\Delta E < 0$) intensities, $(I_b - I_r)/I_b$ (Fig. 1).
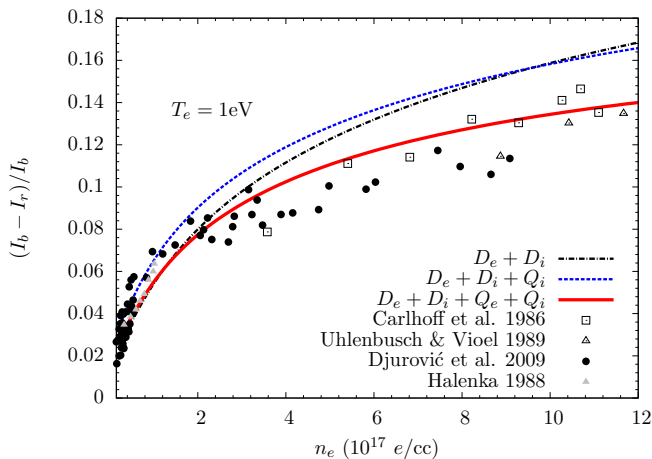

FIG. 2. Asymmetry calculations (lines) with different approximations: dipole-only interaction (black); dipole + ion-quadrupole (blue); dipole + electron- *and* ion-quadrupole moment (red). The dipole-only calculation agrees well with the data (various points) below 3×10^{17} e/cc. Including only ion-quadrupole created discrepancy at these densities. Calculations including both electron- and ion-quadrupole terms created agreement with the data between 10^{17} and 10^{18} e/cc. Models assume 1eV temperature.

Figure 2 includes several measurements of the Hβ asymmetry including Carlhoff *et al.* [23], Halenka [24], Djurović *et al.* [21], and Uhlenbusch and Vioel [25]; we then compare asymmetry simulated with different degrees of completeness in the higher-order terms (i.e., $D_e + D_i$, $D_e + D_i + Q_i$, and $D_e + D_i + Q_e + Q_i$) against the measured asymmetry.

The dipole-only calculation ($D_i + D_e$) compares well

with the measured asymmetry at the density below $\sim 2 \times 10^{17}$ e/cc but over-predicts the asymmetry above this threshold, reproducing the results of the simulation-based line-shape models presented in Djurović *et al.* [21]. The calculation that includes Q_i increases the asymmetry compared with dipole-only calculation, showing less agreement with the data. When we include both Q_i and Q_e, the calculated asymmetry improved and successfully reproduced the measured asymmetry throughout the available n_e data.

We repeated this calculation at 2 eV because the experiments [21, 23–25] have reported temperatures between 1 and 2 eV. All of the calculated asymmetries based on the listed approximations ($D_e + D_i$, $D_e + D_i + Q_i$, and $D_e + D_i + Q_e + Q_i$) systematically increase with temperature. Thus, the calculation with $D_e + D_i + Q_e + Q_i$ at 2 eV temperature still more accurately reproduces the trend seen in the measurements.

This improvement can be explained by the fact that the shape around the line center is more susceptible to rapid microfield fluctuations [26]. Since electrons move much faster than ions, the inclusion of Q_e changes the width of the various Stark components. Thus, to model the line shape accurately throughout the line profile, it is important to consistently include higher-order terms from both ions (Q_i) and electrons (Q_e).

IV. CONVERGENCE OF THE MULTIPOLE EXPANSION

We include multipole terms consistently from both ions and electrons and study how the Hβ line shape converges with higher-order terms. We only explore the line shapes at 1 eV because the relative importance of the higher order multipole terms is not sensitive to temperature.

In Figure 3, we compare the Hβ line shapes calculated with different multipole terms at a) 10^{17}, b) 10^{18}, and c) 10^{19} e/cc. The green, blue, orange, and red represent Hβ line shapes computed with the terms up to the dipole ($k \leq 1$), the quadrupole ($k \leq 2$), the octupole ($k \leq 3$), and the sedecapole ($k \leq 4$), respectively. Figure 3-a) shows all profiles having nearly identical shapes, indicating that the line shape computed with the dipole term is sufficiently accurate at this lower density. In Figure 3-b), the dipole line shape is systematically wider and shorter than the line shape with more-complete calculations. Figure 3-c) shows the opposite trend; the dipole line shape is systematically narrower and taller and shows larger asymmetry. In either case, the quadrupole line shape is consistent with more-complete octupole and sedecapole line shapes.

To quantify the goodness of the dipole and quadrupole line shapes, we compute the average percent error in the line shapes, assuming that the sedecapole profile is the
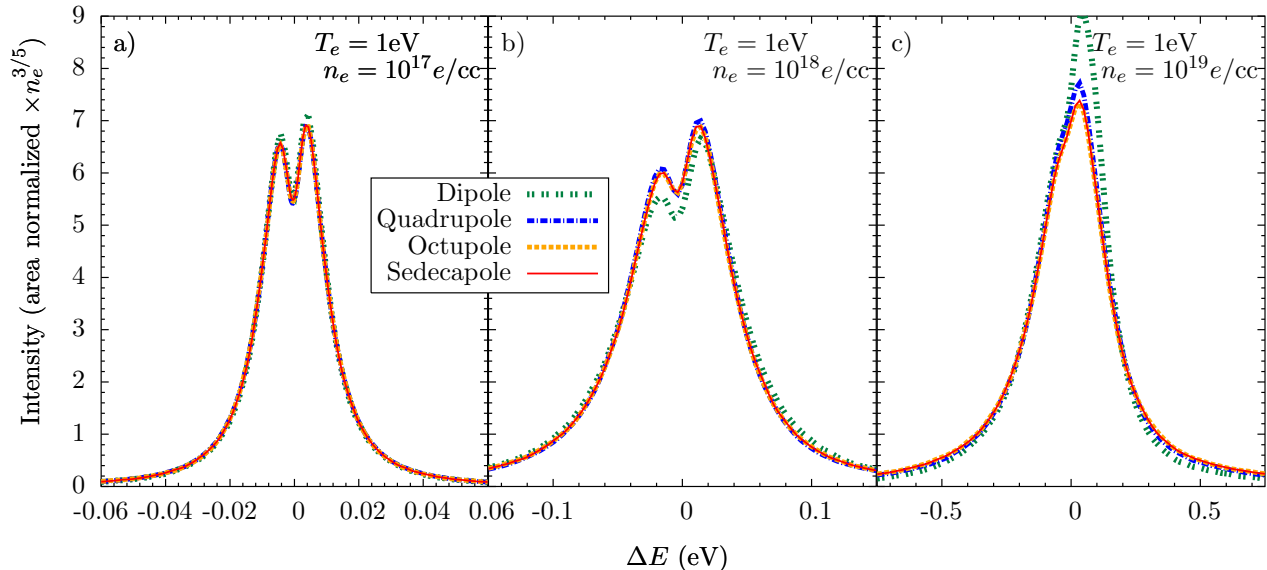
FIG. 3. Area-normalized Hβ profiles at various levels of approximation over several different conditions. Profiles calculated at electron densities of 10^{17}, 10^{18}, and $10^{19} e$/cc are shown (all at 1-eV temperature). All moments include contributions from both ions and electrons. The green line shows the dipole approximation of Eq. (4); blue line shows up to the quadrupole term; orange line shows up to octupole term; lastly, red shows up to the sedecapole ($k \leq 4$) term, indistinguishable from the octupole profile. The profiles that include up to the quadrupole term match reasonably well to the sedecapole profile.

correct one:

$$\text{Percent Error} = \frac{1}{n} \sum_{i=1}^{n} \frac{|\phi(E_i) - \psi(E_i)|}{\psi(E_i)} \times 100\%, \quad (10)$$

where ψ is the sedecapole profile, ϕ is either the dipole or quadrupole profile, and the sum of i is only over points within the energy range of interest. We compare the line-shape accuracy over two energy ranges: the core and wings. The core is defined as the photon-energy range inside the full width at half maximum ($|\Delta E| <$ FWHM), and the wings are defined to have the energy ranges between that and twice the full width at half maximum (FWHM $< |\Delta E| < 2 \times$ FWHM).

Table I summarizes the percent errors of the dipole, quadrupole, and octupole line shapes for the core and wings, respectively. As electron density increases, the error in the dipole line shape significantly increases from less than 1% to nearly 10%, while the quadrupole line shapes are accurate within a few percent throughout the tested densities. The percent error in the octupole line shape is less than 1% across all densities. It is important to include at least up to quadrupole terms to accurately calculate the line shapes within 2% error.

V. DENSITY DIAGNOSTICS

Plasma electron density is often diagnosed by fitting a modeled line shape to the measured line shape. However, many line-shape models used for this purpose employ up

TABLE I. Percent Error in Line Shape

n_e (e/cc)	Dipole	Quadrupole	Octupole	Region
10^{17}	0.53	0.52	0.40	
10^{18}	5.20	0.88	0.58	Core
10^{19}	8.68	2.10	0.89	
10^{17}	0.78	0.80	0.81	
10^{18}	9.2	1.1	0.81	Wings
10^{19}	5.05	1.7	0.80	

to the dipole term (known as the dipole approximation) for the perturber-radiator interaction potential in Eq. 4. Since we find the quadrupole terms are important for accurate line-shape calculation (sec 4), here we investigate the impact of including higher-order multipole terms on density diagnostics.

The black dots in Figure 4-a) and b) are Hβ line profiles measured by Wiese et al. [27] and by Carlhoff et al. [23], respectively. We fit these measured profiles with dipole, quadrupole, and sedecapole line shapes to infer the electron density of the source plasmas. Since the sedecapole line shape includes most higher-order multipole terms, we consider the diagnostics with this line shape to be the most accurate. Based on our sedecapole line-shape diagnostics, the inferred conditions are $n_e = 9.2 \times 10^{16}$ e/cc and 1.5×10^{18} e/cc, respectively. Our determination for Figure 4-a agrees well with the conditions published in [27], which was determined to be 9.3×10^{16} e/cc). However, we note that our inferred density is slightly different for the [23] data (determined to be 1.1×10^{18} e/cc from

Lorentz fitting) since they only compared the FWHM with a calculation from Griem [28].

When we use the dipole and quadrupole line shapes, the inferred conditions are not always consistent with the values inferred while using the sedecapole line-shape model even though the fits always look reasonable. For Figure 4-a), the percent difference in inferred density is 1.6% between the sedecapole and dipole profiles, while that of the quadrupole profile shows half a percent difference.
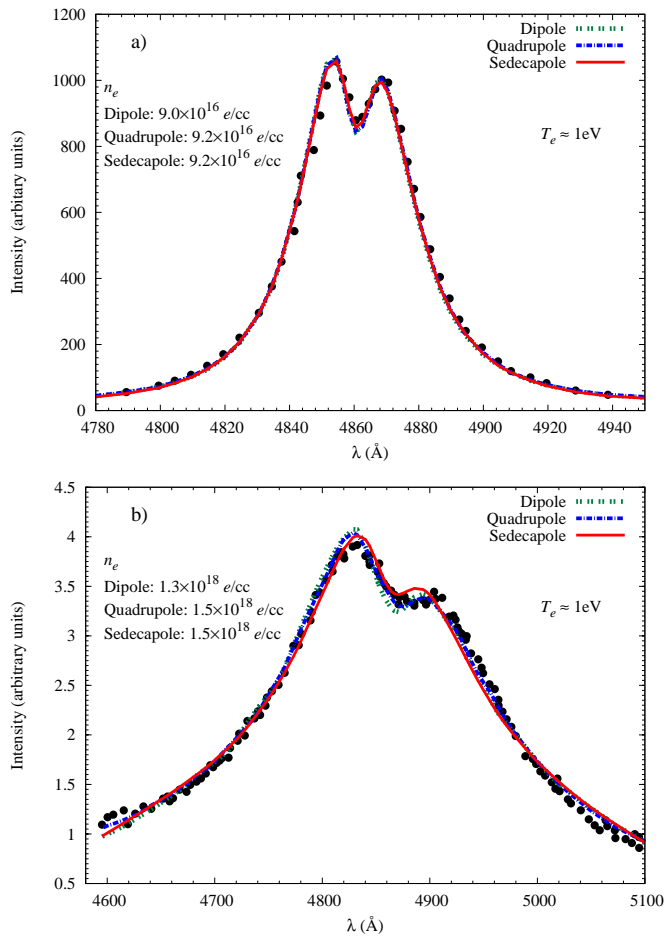

FIG. 4. a) the highest-density measured spectrum from the Wiese *et al.* [27] experiment, focused on Hβ (dots). The fits for the calculated dipole, quadrupole, and sedecapole profiles are identical, yielding fit differences less than the fit errors. b) the measured Hβ spectrum measured by Carlhoff *et al.* [23] (dots). The fits for the calculated dipole, quadrupole, and sedecapole profiles yield differences in density of 12%, which is greater than the fit errors.

In Figure 4-b), we compare a case where electron density is above 10^{18} e/cc. The densities inferred with the dipole and quadrupole line shapes are 1.3×10^{18} e/cc and 1.5×10^{18} e/cc, respectively.

For a quantitative discussion we use $\sum (data - model)^2$, which is similar to the variance, as a measure of the goodness of the fit because the uncertainties on the individual data points are not available; the results are shown in Table II. For the Wiese experiment, our χ^2 decreases for each of the higher-order approximations, while the for Carlhoff experiment, the χ^2 varies between the different approximations rather than steadily decreasing. The trends reported are not conclusive. There could be other sources of error due to neglect of high-density effects, such as the overlapping Hγ line, changes in the relative line intensity, the lowered continuum, and the disappearance of substates; these effects are beyond the scope of this paper.

TABLE II. $\sum (data - model)^2$ (Intensity Units)

Approximation	Wiese	Carlhoff
Dipole	1166	9.9×10^{-3}
Quadrupole	860	5.1×10^{-3}
Sedecapole	829	9.5×10^{-3}

At these high densities, the dipole line shape becomes inaccurate as discussed in Sec. IV and underestimates the density by 12%, while the quadrupole line shape still infers the correct density. At these densities, including quadrupole terms is necessary for accurate electron-density diagnostics.

VI. CONCLUSIONS

We explore the higher-order multipole moments in the Coulomb interaction potential between the radiator and the perturbing particles, focusing on their effect on line shapes. While this is important for all line-shape theory, we focus on the hydrogen Balmer β line ($n = 4 \rightarrow 2$) due to its use as an astrophysical and laboratory diagnostic [3]. This is the first line-shape calculation to include higher-order multipole moments from both ions and electrons in the plasma. In calculations of the asymmetry of the Hβ line, the quadrupole term due to the ions is often included while the quadrupole term due to the electrons is usually neglected. We show that including just the ions in the quadrupole calculation results in greater disagreement with measurement, while including quadrupole contributions from *both* ions and an electrons brings the asymmetry into agreement with data. We also study the convergence of the line shapes from using the higher-order multipole moments; at least quadrupole term should be included for two percent accuracy in the line shape. Using line shapes calculated up to the dipole term infer erroneous electron densities at $n_e \geq 10^{18} e$/cc, while using the quadrupole profile is in error of 2% or less at densities up to the Inglis-Teller limit of the Hβ line ($\sim 10^{19}$ e/cc). The line-shape inaccuracy due to omitting the quadrupole terms would cause one to underestimate the density inferred from a measured spectrum by $\sim$12% even at a density as low as 10% of its Inglis-Teller limit. While we focus on the Hβ line-shape calculation, similar impact is expected from other lines.

We therefore find that it is necessary to include up to at least the quadrupole terms due to *both* the ions and electrons for accurate line-shape calculations and accurate electron-density diagnostics.

[1] M. A. Gigosos and V. Cardeñoso, Journal of Physics B Atomic Molecular Physics **29**, 4795 (1996).

[2] C. Stehlé, M. Busquet, D. Gilles, and A. V. Demura, Laser and Particle Beams **23**, 357 (2005).

[3] R. E. Falcon, G. A. Rochau, J. E. Bailey, T. A. Gomez, M. H. Montgomery, D. E. Winget, and T. Nagayama, Astrophys. J. **806**, 214 (2015), arXiv:1505.03801 [astro-ph.SR].

[4] R. D. Cowan, *The Theory of Atomic Structure and Spectra, Los Alamos Series in Basic and Applied Sciences* (University of California Press, Berkeley, 1981).

[5] H. A. Bethe and E. E. Salpeter, *Quantum Mechanics of One- and Two-Electron Atoms* (New York: Academic Press, 1957).

[6] P. Kepple and H. R. Griem, Physical Review **173**, 317 (1968).

[7] C. R. Vidal, J. Cooper, and E. W. Smith, J. Quant. Spec. Radiat. Transf. **11**, 263 (1971).

[8] M. A. Gigosos and V. Cardenoso, Journal of Physics B Atomic Molecular Physics **20**, 6005 (1987).

[9] E. Stambulchik and Y. Maron, J. Quant. Spec. Radiat. Transf. **99**, 730 (2006).

[10] D. P. Kilcrease, R. C. Mancini, and C. F. Hooper, Jr., Phys. Rev. E **48**, 3901 (1993).

[11] A. V. Demura, D. Gilles, and C. Stehlé, in *American Institute of Physics Conference Series*, American Institute of Physics Conference Series, Vol. 386 (1997) pp. 119–120.

[12] W. Olchawa, J. Quant. Spec. Radiat. Transf. **74**, 417 (2002).

[13] L. A. Woltz and C. F. Hooper, Jr., Phys. Rev. A **30**, 468 (1984).

[14] G. C. Junkel, M. A. Gunderson, C. F. Hooper, Jr., and D. A. Haynes, Jr., Phys. Rev. E **62**, 5584 (2000).

[15] D. R. Inglis and E. Teller, Astrophys. J. **90**, 439 (1939).

[16] P. W. Anderson, Physical Review **76**, 647 (1949).

[17] T. A. Gomez, *Examining Line Broadening Approximations using Xenomorph: A Simulation Line Broadening Program*, Master's thesis, University of Texas at Austin (2013).

[18] S. Ferri, A. Calisti, C. Mossé, J. Rosato, B. Talin, S. Alexiou, M. Gigosos, M. González, D. González-Herrero, N. Lara, T. Gomez, C. Iglesias, S. Lorenzen, R. Mancini, and E. Stambulchik, Atoms **2**, 299 (2014).

[19] M. Baranger, Physical Review **111**, 481 (1958).

[20] E. Stambulchik, D. V. Fisher, Y. Maron, H. R. Griem, and S. Alexiou, High Energy Density Physics **3**, 272 (2007).

[21] S. Djurović, M. Ćirišan, A. V. Demura, G. V. Demchenko, D. Nikolić, M. A. Gigosos, and M. Á. González, Phys. Rev. E **79**, 046402 (2009).

[22] H. R. Griem, *Spectral Line Broadening by Plasmas* (New York: Academic Press, 1974).

[23] C. Carlhoff, E. Krametz, J. H. Schaefer, and J. Uhlenbusch, Journal of Physics B Atomic Molecular Physics **19**, 2629 (1986).

[24] J. Halenka, J. Quant. Spec. Radiat. Transf. **39**, 347 (1988).

[25] J. Uhlenbusch and W. Vioel, Contributions to Plasma Physics **29**, 459 (1989).

[26] S. Alexiou, High Energy Density Physics **5**, 225 (2009).

[27] W. L. Wiese, D. E. Kelleher, and D. R. Paquette, Phys. Rev. A **6**, 1132 (1972).

[28] H. R. Griem, *Plasma spectroscopy* (New York: McGraw-Hill, 1964).